ELSEVIER

Physica C 350 (2001) 276–290

PHYSICA C

www.elsevier.nl/locate/physc

Influence of the transparency of tunnel barriers in $Nb/Al_2O_3/Al/Al_2O_3/Nb$ junctions on transport properties

D. Cassel [a], G. Pickartz [a], M. Siegel [a,*], E. Goldobin [a], H.H. Kohlstedt [b], A. Brinkman [c], A.A. Golubov [c], M.Yu. Kupriyanov [d], H. Rogalla [c]

[a] *Institut für Schicht und Ionentechnik, Forschungszentrum Jülich GmbH, Jülich 52425, Germany*

[b] *Institut für Elektrokeramik, Forschungszentrum Jülich GmbH, Jülich 52425, Germany*

[c] *Department of Applied Physics, University of Twente, P.O. Box 217, 7500 AE, The Netherlands*

[d] *Institute of Nuclear Physics, Moscow State University, 119899 Moscow, Russia*

Received 17 April 2000; received in revised form 26 September 2000; accepted 28 September 2000

Abstract

The transparency of the tunnel barriers in double-barrier junctions influences the critical current density and the form of the current–voltage characteristics (IVC). Moreover, the barrier asymmetry is an important parameter, which has to be controlled in the technological process. We have performed a systematic study of the influence of the barrier transparency on critical current, I_C, and normal resistance, R_N, by preparing SIS and SINIS junctions under identical technological conditions and comparing their transport properties. We have fabricated $Nb/Al_2O_3/Nb$ and $Nb/Al_2O_3/Al/Al_2O_3/Nb$ devices with different current densities using a conventional fabrication process, varying pressure and oxidation time. The thickness of the Al middle electrode in all $Nb/Al_2O_3/Al/Al_2O_3/Nb$ junctions was 6 nm. Patterning of the multilayers was done using conventional photolithography and the selective niobium etching process. The current density of SIS junctions was changed in the range from 0.5 to 10 kA/cm^2. At the same conditions the current density of SINIS devices revealed 1–100 A/cm^2 with non-hysteretic IVC and characteristic voltages, $I_C R_N$, of up to 200 μV. By comparing the experimental and theoretical temperature dependence of the $I_C R_N$ product we estimated the barrier transparency and its asymmetry. The comparison shows a good agreement of experimental data with the theoretical model of tunneling through double-barrier structures in the dirty limit and provides the effective barrier transparency parameter $\gamma_{eff} \approx 300$. A theoretical framework is developed to study the influence of the barrier asymmetry on the current–phase relationship and it is proposed to determine the asymmetry parameter by measuring the critical current suppression as function of applied microwave power. The theoretical approach to determine the non-stationary properties of double-barrier junctions in the adiabatic regime is formulated and the results of calculations of the I–V characteristics are given in relevant limits. The existence and the magnitude of a current deficit are predicted as function of the barrier asymmetry. © 2001 Elsevier Science B.V. All rights reserved.

Keywords: Josephson junctions; Integrated circuits; Double-barrier; Tunneling

1. Introduction

Applications of Josephson junctions in integrated circuits for rapid-single-flux quantum

* Corresponding author.
E-mail address: m.siegel@fz-juelich.de (M. Siegel).

0921-4534/01/$ - see front matter © 2001 Elsevier Science B.V. All rights reserved.
PII: S0921-4534(00)01613-0

(RSFQ) logic and voltage calibrators require devices with non-hysteretic current–voltage characteristics (IVC). Standard $Nb/Al_2O_3/Nb$ tunnel junctions should be shunted with an external shunt to achieve a value of the McCumber parameter $\beta_C < 1$. External shunts reduce the characteristic voltage of Josephson junctions and have large dimensions of about 10 to 50 μm and require additional wiring. One concept to achieve non-hysteretic IVC is to increase the Josephson current density, J_C, above 10^2 kA/cm^2 [1,2]. Another approach is to use intrinsically shunted SINIS structures with a middle electrode consisting of a thin Al layer [3–18].

From our point of view the last approach is more attractive for several reasons. The main advantage of the double-barrier junctions is the availability of two self-averaging mechanisms that make the structure very reproducible and technologically feasible. The first mechanism is provided by the existence of two barriers in the structure. This makes the probability to have a shunting via a pinhole through both barriers extremely small. The second mechanism is based on the large coherence length of the Al interlayer. It realizes an averaging of the spatial variations of the superconducting parameters in Al caused by inhomogeneities in the barriers transparency and deterioration of local junction parameters in the areas close to the outer perimeter of the structure, which can arise during the fabrication process. Additionally, double-barrier junctions are intrinsically shunted by a resistor with very small voltage dependence [19]. They have IVC very close to those described by the RSJ model. Finally the structures $NbAl/Al_2O_3/Al/Al_2O_3/Nb$ (SIS′IS) can be fabricated with relatively small modifications of existing conventional facilities for fabricating $Nb/Al_2O_3/Nb$ tunnel devices.

At PTB, SINIS junctions have been successfully implemented in Josephson voltage standard circuits. A high level of complexity has been reached by integrating up to 70 000 Josephson junctions [20]. A 10 V constant voltage step has been reached showing that the parameter spread of the SINIS junctions was rather small.

Two important parameters of SIS′IS junctions are the critical temperature of the S′ interlayer and the suppression parameter γ_{eff} [5] which is mainly controlled by the transparency of the interfaces. We have performed a systematic study of the influence of the barrier transparency on critical current, I_C, and normal resistance, R_N, by preparing SIS and SINIS junctions under identical technological conditions and comparing their transport properties.

It is important to note that the advantages of SIS′IS structures can be used to improve the reproducibility of SIS devices, especially in the case of small critical current densities. It is sufficient to prepare SIS′IS structures with barriers having a one order of magnitude different interface transparency. In this case a simple method for estimation of the level of asymmetry of the transparency is needed.

In this paper we have performed a systematic study of the influence of the barrier transparency on critical current, I_C, and normal resistance, R_N, by preparing SIS and SINIS junctions under identical technological conditions and comparing their transport properties. The influence of the barrier asymmetry on the current–phase relationship is modeled and it is proposed to determine the asymmetry parameter by measuring the critical current suppression as function of applied microwave power. We will discuss the non-stationary current of double-barrier junctions by focusing on the quasi-particle current at high and low voltage bias. The existence of a current deficit is derived and the influence of the asymmetry parameter on this current deficit is studied.

2. Fabrication

We have fabricated $Nb/Al_2O_3/Nb$ and $Nb/Al_2O_3/Al/Al_2O_3/Nb$ devices using the conventional selective niobium anodization process (SNAP) [21]. The multilayer $Nb/Al_2O_3/Al/Al_2O_3/Nb$ or $Nb/Al_2O_3/Nb$ were deposited on an cooled oxidized 2-in. Si wafer by dc sputtering with a base pressure less than 10^{-6} mbar. The thickness of the Nb base and top electrodes are 100 and 30 nm, respectively. The thickness of the Al middle electrode was 6 nm and was kept constant. The tunnel barriers were formed by thermal oxidation in pure

oxygen at room temperatures. Oxidation is the crucial step in the fabrication process of double-barrier structures. The exposure parameter *pt* (where *p* is the oxygen pressure in the chamber and *t* the oxidation time of the Al layers) commonly used for barrier fabrication must have extremely small values [6,11,12,16,18]. To achieve different current densities the pressure and oxidation time have been changed from 10^{-3} to 10^{-1} mbar and 1–30 min, respectively. The oxidation was performed in the deposition chamber and for both barriers under identical conditions. The main disadvantage of this approach is that the residual oxygen pressure in the chamber may play a significant role for the success of the whole fabrication process. In particular, it may influence the critical temperature T_C^* of the Al interlayer, increasing sometimes its value to about 2.7 K [17]. The increase of T_C^* is a consequence of changes in the transport properties of thin interlayer Al. The larger is T_C^*, the closer the film to the dirty limit conditions. Differences in the crystalline structure and surface morphology between the first Al layer deposited on the base Nb electrode and the second interlayer Al layer deposited on the lower Al_2O_3 barrier may cause changes in the growth of the first and second Al_2O_3 barriers even if they are grown under the same thermodynamic conditions. Thus we may have a difference in the transparency of both tunneling barriers, which is difficult to control. To minimize these influences we have used a Nb pre-sputtering step to reduce partial pressure of oxygen before deposition of the next layer. Additionally we have changed our standard SIS fabrication process. In the SINIS fabrication process the oxidation process is performed in a continuous oxygen gas flow. This makes short oxidation times, exact pressure control, and low desorption rates of residual gases possible.

The patterning of all devices has been performed by conventional contact photolithography. Fig. 1 shows the main steps of our fabrication process. To prepare the base electrode the $Nb/Al_2O_3/Al/Al_2O_3/Nb$ or $Nb/Al_2O_3/Nb$ multilayer was patterned by lift-off. Then the wafers were anodized. The anodization was stopped at voltages of 47 V. Afterwards the 300 nm thick top electrode and wiring layer were deposited by dc sputtering and patterned by lift-off.

The electrical measurements were performed by standard four-point measurements with a PC based data acquisition system. The measurements of temperature dependencies of the critical current in the range of 0.3–8 K have been made in He^3 cryostat. The dependencies of the critical currents and normal resistances of SIS and SINIS junction fabricated under the same technological conditions are shown in Fig. 2.

3. Experimental results

Single SIS and SINIS Josephson junctions covering a large variety of different areas have been fabricated and tested. Fig. 3a–c shows IVC and the magnetic field dependence of critical cur-

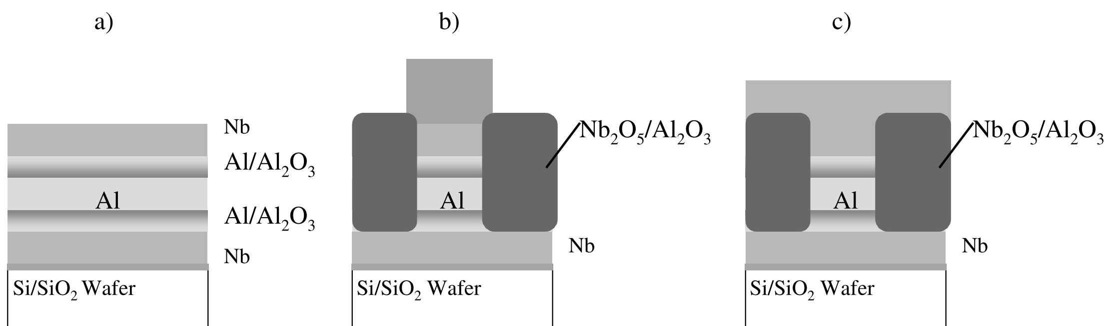

Fig. 1. Schematic illustration of the fabrication process of SINIS Josephson junctions made from (a) a $Nb/Al_2O_3/Al/Al_2O_3/Nb$ trilayer, (b) patterned by the selective anodization process and (c) finalized with a Nb wiring layer.

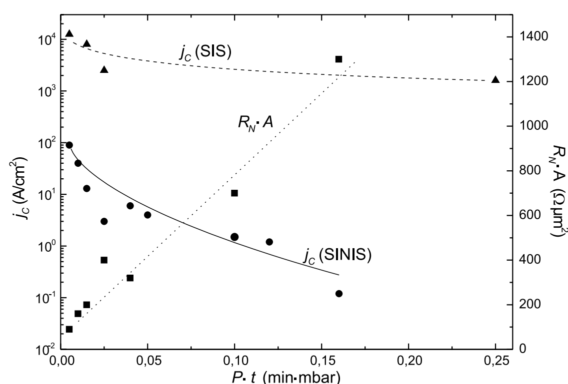

Fig. 2. Dependence of the critical current density j_C of SIS and SINIS junctions with a 6 nm thick Al interlayer and of the normal resistance R_NA on pt product.

rent, $I_C(H)$, of a SIS junction at $T = 4.2$ K. The critical current of the single junction in Fig. 3(a) is found to be $I_C = 5.3$ mA ($j_C = I_C/A = 663$ A/cm^2, $A = 800$ μm^2) and its characteristic voltage to be $V_C = I_CR_N = 1.4$ mV ($R_N = 0.26$ Ω). The junctions with larger critical current density $j_C = I_C/A = 2$ kA/cm^2, $A = 100$ μm^2 often show overheating effects at gap voltages as seen in Fig. 3(b) even at 4.2 K. The magnetic field dependence of critical current behaves classically in external magnetic field H as shown in Fig. 3(c) demonstrating a high degree of homogeneity of the supercurrent distribution in the cross-section of the tunnel barrier. We have fabricated SIS junctions with different current densities in the range of (0.1–10) kA/cm^2 by changing the pt-product between 1 and 10^{-2}) min mbar, where p is the oxygen pressure and t is the oxidation time.

Based on these results, we have fabricated double-barrier devices under the same deposition and oxidation conditions as SIS junctions. At $T = 4.2$ K all junctions exhibit a nearly hysteretic-free IVC. The hysteresis is less than 10% as shown in Fig. 4a–d. The hysteresis is defined as $(I_C - I_{RET})/I_C$ where I_{RET} is the return current. As seen in Fig. 4a and b at small voltages, $eV \leqslant \Delta_{Nb}/\gamma_{eff} \ll \Delta_{Nb}$ the IVC looks rather similar to the IVC predicted by the RSJ model. At larger voltages the dc current across the structures becomes

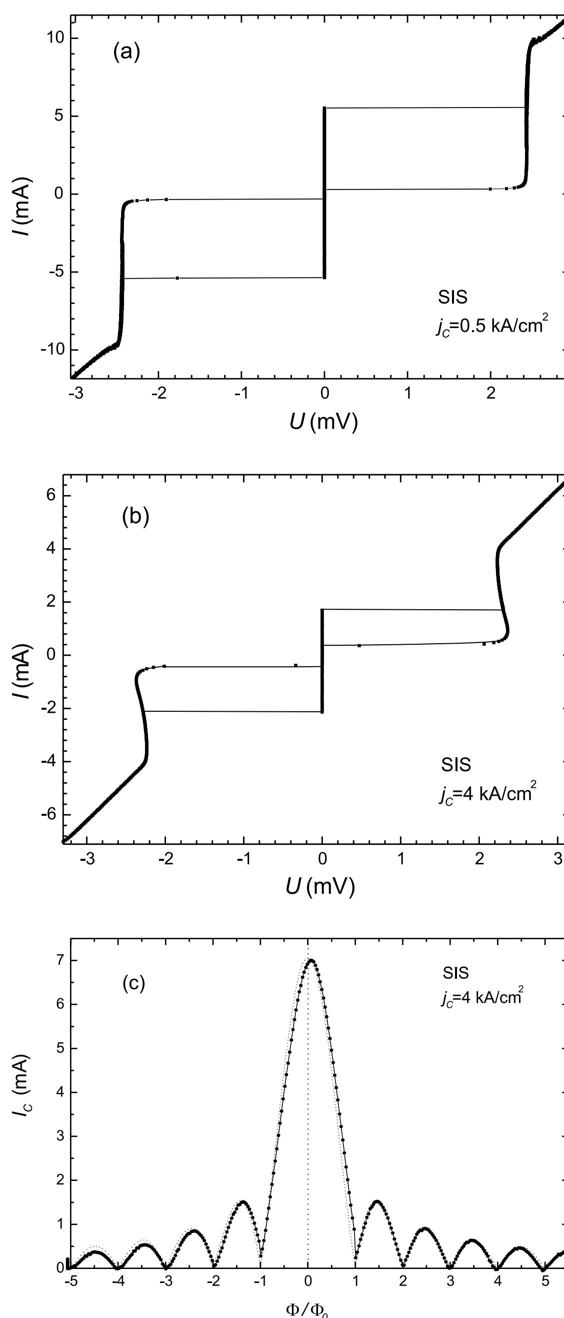

Fig. 3. (a) Typical IVC of a SIS junction with a current density of $j_C = 500$ A/cm^2 at $T = 4.2$ K. (b) Typical IVC of a SIS junction with a current density of $j_C = 4$ kA/cm^2 at $T = 4.2$ K. (c) Magnetic field dependence of critical current of a typical SIS junction with $j_C = 4$ kA/cm^2 at $T = 4.2$ K.

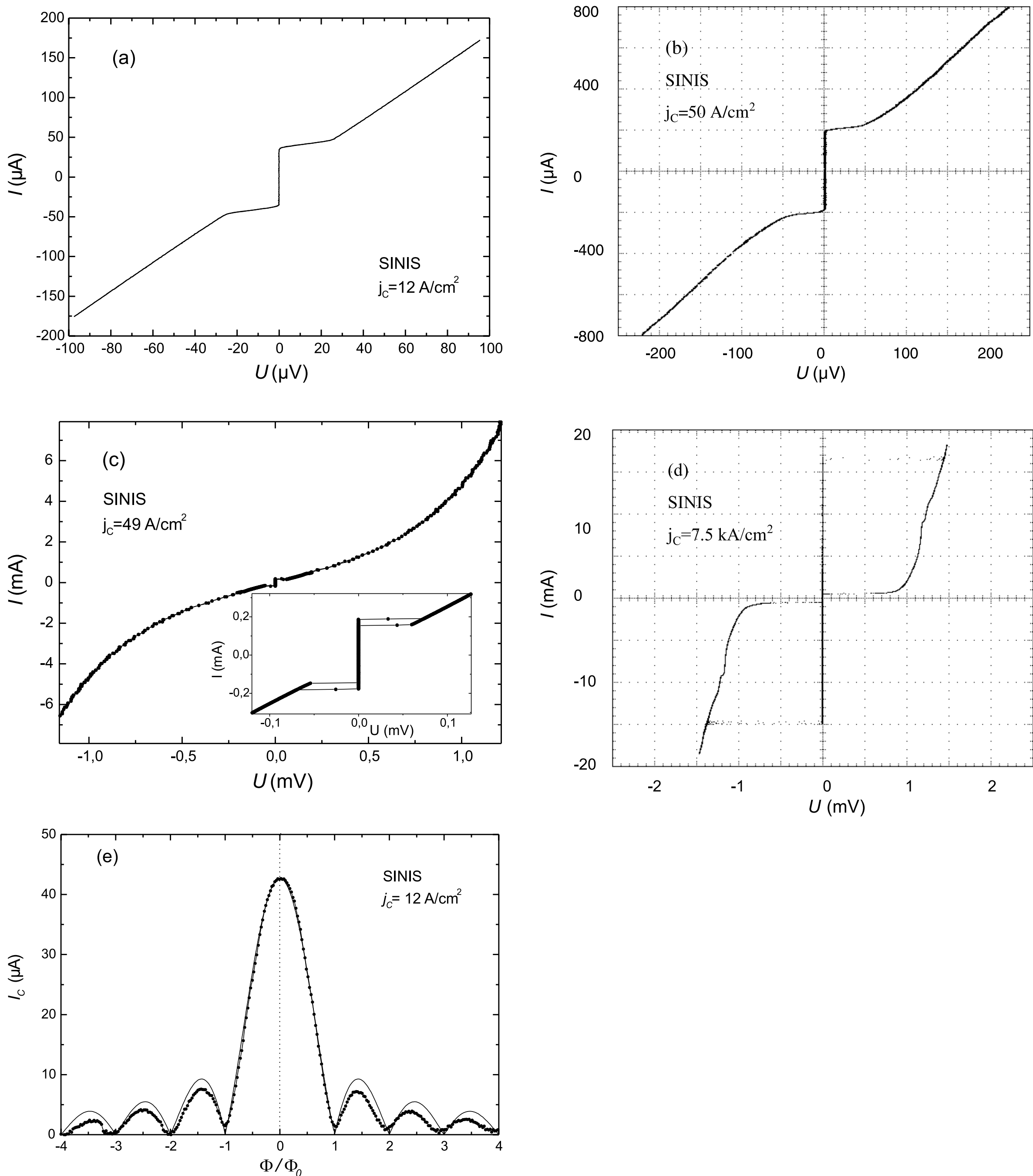

Fig. 4. (a) IVC of a SINIS junction with a critical current density of $j_C = 12$ A/cm^2 at $T = 4.2$ K. (b) IVC of a SINIS junction with a critical current density of $j_C = 50$ A/cm^2 at $T = 5.8$ K (x-axis: 50 μV/div, y-axis: 200 μA/div). (c) IVC of a SINIS junction with a critical current density of $j_C = 49$ A/cm^2 at $T = 4.2$ K. The inset shows the small hysteresis close to the critical current for small voltages. (d) IVC of a SINIS junction with a critical current density of $j_C = 7.5$ kA/cm^2 at $T = 0.5$ K (x-axis: 500 μV/div, y-axis: 5 mA/div). (e) Magnetic field dependence of critical current of a typical SINIS junction with $j_C = 12$ A/cm^2 at $T = 4.2$ K.

a non-linear function of applied voltage with a strong increase of current at $eV \propto \Delta_{Nb}$ as shown in Fig. 4c and d. It demonstrates that in this voltage range the junction behaves like a single SIN junction.

It is important to note that the spread of critical currents of double-barrier junctions on a wafer was practically half an order of magnitude smaller compared to the spread of SIS devices. The on-chip spread of SINIS devices reaches about 3%. The chip-to chip spread is significantly higher as seen in Fig. 2. The deviations of their $I_C(H)$ dependence from the well known Fraunhofer pattern [Fig. 4(e)] is also practically negligible.

4. Determination of the suppression parameter

In the frame of the microscopic theory of superconductivity it was shown [3–5] that for a small interlayer thickness d (compared to its decay length ξ_{nd}) the supercurrent $I(\varphi)$ across an SIS′IS structure has the form

$$\frac{I(\varphi)R_N}{2\pi T_C} = \frac{T}{T_C\gamma_{eff}}\left\{\sum_{\omega>0}\frac{f^2}{\omega^2+f^2}\frac{\pi T_C}{\Omega}\right\}\sin(\varphi) + \frac{T}{T_C}\left\{\sum_{\omega>0}\frac{f}{\sqrt{\omega^2+f^2}}\frac{\Delta}{\Omega}\right\}\frac{\sin(\varphi)}{\eta(\phi)}, \quad (1)$$

where

$$\Omega = \sqrt{\omega^2(1+q)^2 + (fq\eta(\varphi)+\Delta)^2},$$
$$\eta(\varphi) = \sqrt{\cos^2(\varphi) + \gamma_-^2\sin^2(\varphi)}, \quad (2)$$

$$q = \frac{\pi T_C g}{\omega\gamma_{eff}}, \qquad \gamma_- = \frac{\gamma_{B1}-\gamma_{B2}}{\gamma_{B1}+\gamma_{B2}}. \quad (3)$$

Here f and g are the absolute values of Green's functions in the superconducting banks, $\omega = \pi T(2n+1)$ are the Matsubara frequencies and Δ is the modulus of the order parameter of the interlayer which should satisfy the self-consistency equation

$$\Delta\left\{\ln\frac{T}{T_C^*} + 2\pi T\sum_{\omega>0}\left[\frac{1}{\omega}-\frac{1}{\Omega}\right]\right\} = 2\pi T\sum_{\omega>0}\left[\frac{fq\eta(\varphi)}{\Omega}\right]. \quad (4)$$

Here T_C^* is the critical temperature of the interlayer material.

The parameter γ_{eff} describes the overall resistance of the structure and characterizes its $I_C R_N$ product. It is defined by:

$$\gamma_{eff} = \frac{\gamma_{B1}\gamma_{B2}}{\gamma_{B1}+\gamma_{B2}}\frac{d}{\xi_{nd}}, \qquad \xi_{nd} = \sqrt{\frac{D}{\pi T_C}},$$
$$\gamma_{B1,2} = \frac{R_{B1,2}}{\rho_N\xi_{nd}}. \quad (5)$$

Here, $D = v_F l/3$ and ρ_N are correspondingly the diffusion coefficient (v_F is Fermi velocity, l is electron mean free path) and resistivity of the S′-interlayer, T_C is the critical temperature of the S electrodes, $R_{B1,2}$ are the specific boundary resistances at the interfaces between S and S′ electrodes.

The most straightforward way for determination of the suppression parameter is to make a comparison between the theoretical curves following from Eqs. (1)–(4) and the experimental data. The result of this comparison is shown in Figs. 5 and 6.

Fig. 5 shows an overview of the values of the suppression parameter γ_{eff}, deduced from data reported by different research groups [6–14] and including our results. The smallest value of the suppression parameter was achieved in Ref. [18]. In the technology process developed in Refs. [15,16,18] both oxidation processes of Al has been performed in a separate vacuum chamber that is connected with the deposition chamber by a vacuum load-lock system. All other data have been obtained from samples that have been prepared with an oxidation process in the main deposition chamber. From our point of view the technological processes developed in Refs. [6–10,17] leads to relatively high suppression parameters of $\gamma_{eff} > 1000$ and correspondingly to low values of the $I_C R_N$ product of about some tens of microvolts at 4.2 K because of the difficulties in controlling the second oxidation process. There are two

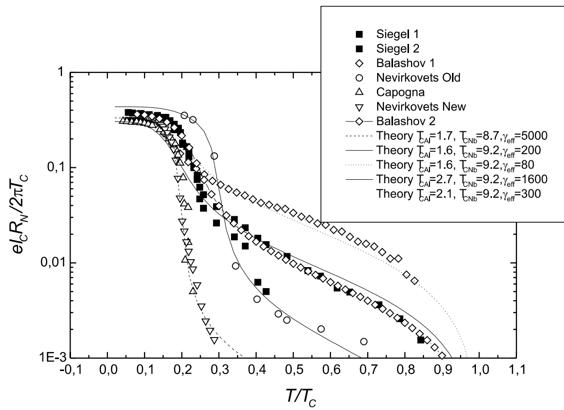

Fig. 5. Temperature dependencies of normalized $I_C R_N$ product of SIS′IS junctions (solid curves) calculated numerically from Eqs. (1)–(5) for different values of the suppression parameter and critical temperatures of interlayer Al and Nb electrodes. The symbols are experimental data obtained at different laboratories. The correlation between our data and those obtained in Ref. [18] is clearly seen.

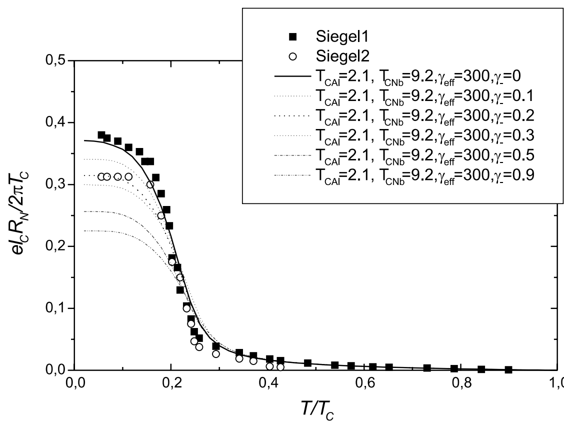

Fig. 6. Temperature dependencies of normalized $I_C R_N$ product of SIS′IS junctions (solid curves) calculated numerically from Eqs. (1)–(5) for different values of the asymmetry parameter and fixed values of critical temperatures of interlayer Al and Nb electrodes and suppression parameter. The symbols are the experimental data. It is seen that asymmetry parameter can be as large as 0.2.

important factors that are necessary to take into account during the second oxidation.

The first of them is the difference in crystalline structure and morphology between the second and first Al layers. The first Al film wets the Nb electrode and has a rather flat surface. The second Al is deposited on its own oxide and must have a rougher surface compared to the first Al layer. The large critical temperature of the second Al film directly show that the transport properties and hence the crystallinity of the first and second Al are different. It means that performing the oxidation of the Al films under the same oxidation conditions we may get barriers with different transparencies.

The second factor is the long relaxation process of switching on and off the oxidation in the deposition chamber. This factor is not very important if we want to fabricate structures with small critical current densities. But if we are interested in relatively high-J_C devices we have to reduce these times to values at least an order of magnitude smaller than the oxidation time. This is difficult to achieve in technologies developed in Refs. [6–10,17].

Our data, shown in Fig. 5, which can be fitted well with a suppression parameter of $\gamma_{\mathrm{eff}} \approx 300$ are rather close to those obtained at PTB ($\gamma_{\mathrm{eff}} \approx 80$–300) [18]. It means that in our technological process the second factor is not as important as in Refs. [6–10,17]. Therefore we assume that in our case as well as in Ref. [18] the parameters of the second tunnel barrier are more dependent on the properties of the Al layer like crystalline structure and morphology rather than on external oxidation conditions. Fig. 6 illustrates the influence of a difference in the barriers transparencies of the two tunneling barriers. The solid lines in Fig. 7 are the results of numerical calculations for the following set of the parameters $T_C = 9.2$ K, $T_C^* = 2.1$ K, $\gamma_{\mathrm{eff}} = 300$. The asymmetry parameter γ_- changes from 0 to 1. It is interesting that changes of γ_- influence the shape of $I_C(T)$ mainly at temperatures smaller T_C^* . In the limit of large asymmetry ($\gamma_- \to 1$) calculations reproduce the results obtained for SS′IS tunnel junctions [22]. The data for sample shown in Fig. 6 can be fitted reasonably well by the theoretical curve calculated with an asymmetry of $\gamma_- = 0$ and 0.2.

This result as well as the rather large value of the critical temperature of the Al layer may be explained by the fact that the oxidation process in the deposition chamber influences not only the

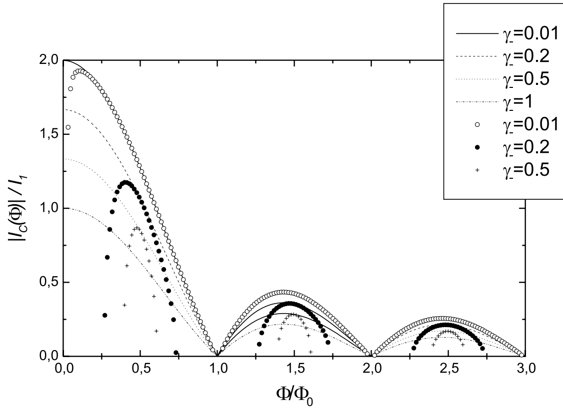

Fig. 7. Magnetic field dependence of critical current calculated numerically at $T \ll T_C$ from Eq. (10) for different values of the asymmetry parameter γ_-. Solid and dotted lines correspond to "0–0–0" and "0–π–0" states.

transport properties of the intermediate Al layer by making it more dirty and therefore increasing T_C^* and suppressing the decay length. It also changes the conditions of the second oxidation process because the quality of first and second Al layers should be different.

Nevertheless, from Fig. 6 it is clearly seen that in the practically interesting interval of operating temperatures $T = 4.2$ K the influence of asymmetry on $I_C R_N$ is negligible in the limit of large γ_{eff}. On the other hand, the increase of the asymmetry leads to changes in the form of the IVC of the devices. The direct way for experimental determination of the asymmetry parameter are measurements of the resistance of the individual barriers using an intermediate electrode with a contact to an external current supply. It is also possible to estimate γ_- indirectly using deviations of $I(\varphi)$ relation from the sinusoidal form.

5. Current–phase relationship

From Eqs. (1) and (2) in the extremely asymmetric case ($\gamma_- = 1$) it follows that the parameter $\eta = 1$ and the $I(\varphi)$ relationship has a $\sin(\varphi)$ form at any values of the suppression parameter. Practically it means that instead of double-barrier device in this limit we really have SS′IS tunnel junction with a complex SS′ electrode. The properties of these structures have been intensively studied [22]. In particular, it is well known that in contrast to symmetric double-barrier structures there is a large hysteresis in the small voltage region on their IVC. Thus, the asymmetry in the barrier properties in SIS′IS junctions is an important parameter which should be effectively controlled. Below we will show that in contrast to $I_C(H)$ measurements the analyses of the I_C suppression as function of applied microwave power provides a very simple and effective tool for experimental determination of the asymmetry parameter γ_-.

5.1. Limit of low temperatures $T \ll T_C^*$

In the limit $T \ll T_C^*$ and $T_C \ll \gamma_{\text{eff}} T_C^*$ Eqs. (1)–(4) reduce to the expression for structures consisting of two SIS′ junctions in series [5]

$$\frac{I(\varphi)R_N}{2\pi T_C} = \frac{T}{T_C}\left\{\sum_{\omega>0}\frac{f}{\sqrt{\omega^2+f^2}}\frac{\Delta}{\sqrt{\omega^2+\Delta^2}}\right\}\frac{\sin(\varphi)}{\eta(\varphi)} = I_0\Psi_0(\varphi),$$
$$\Psi_0(\varphi) = \frac{\sin(\varphi)}{\eta(\varphi)}. \tag{6}$$

The analytical form of $I(\varphi)$ opens the possibility to study the influence of external magnetic and microwave fields on junctions parameters without a numerical solution of the whole set of Eqs. (1)–(4).

5.1.1. Fraunhofer pattern

In our approach it was supposed that the width of the structure is much smaller than the Josephson penetration depth. For this reason in an external magnetic field H the phase difference in Eq. (6) scales linearly with the field H

$$\varphi = 2hx + q, \quad h = \frac{\pi\Phi}{\Phi_0}, \tag{7}$$

where Φ_0 is magnetic flux quantum and Φ is the external magnetic flux. The critical current of the junction has to be found as

$$I_C = I_0 \max_q \left\{ \int_0^1 \Psi_0(\varphi)\, dx \right\}. \tag{8}$$

It can be shown that the maximum in Eq. (8) is achieved at

$$q_{1,2} = -h \pm \arccos\left\{ \frac{k}{1+\sqrt{1-k^2}} \cos(h) \right\},$$
$$k = \frac{1-\gamma_-^2}{1+\gamma_-^2}, \tag{9a}$$

$$q_{3,4} = -h \pm \text{across}\left\{ -\frac{1+\sqrt{1-k^2}}{k} \cos(h) \right\} \tag{9b}$$

and is equal to

$$\frac{I_C}{I_0} = \frac{\sin(h)}{h}\Theta(q,h),$$
$$\Theta(q,h) = \frac{2\sqrt{2}}{\sqrt{1+\gamma_-^2}} \times \frac{\sin(q+h)}{\sqrt{1+k\cos q} + \sqrt{1+k\cos(q+2h)}}. \tag{10}$$

In the asymmetric case ($\gamma_- = 1,\ k = 0$) only solution (9a) exists. Substitution of Eq. (9a) into Eq. (10) gives $\Theta(q,h) = 1$ and Eq. (10) reduces to the well-known Fraunhofer pattern. In the opposite situation ($\gamma_- = 0,\ k = 1$) and $q_1 = q_2$. In this limit $\Theta(q,h) = 2$ and we again obtain the Fraunhofer pattern for $I_C(H)$. For arbitrary values of γ_- the $I_C(H)$ dependence have been calculated numerically (see Fig. 7).

There are two sets of curves for $I_C(H)$. The first is obtained by substitution of Eq. (9a) into the expression for critical current (Eq. (10)). The solution (9a) exists at arbitrary values of H and describes the behavior of the structure when the phase of the order parameter of the S′ superconductor at zero magnetic field equals the phase of the electrodes ("0–0–0" state). It is interesting that not only the positions of zeros, but also the form of the curve is independent of γ_- and coincides with the Fraunhofer pattern.

The second set of curves describes the "0–π–0" state. This situation may be realized when the transition into superconducting state occurs in the presence of magnetic fields, which may stabilize the "0–π–0" state. It is interesting that with increasing symmetry of the SIS′IS structure ($\gamma_- \to 0$) the interval of magnetic field in which the critical currents for the "0–0–0" and "0–π–0" states are identical is increased and at $\gamma_- = 0$ these two states may exist at any field.

5.1.2. Shapiro steps

We suppose that at bias current I the dc voltage across the junction is equal to V_0. Therefore the presence of microwave irradiation $V_1 \cos\omega t$ and dc voltage V_0 at the time causes a dependence of the phase difference across the junction in the form

$$\varphi(t) = \frac{2\pi V_0}{\Phi_0} t + \frac{2\pi V_1}{\Phi_0 \omega} \sin(\omega t + \alpha), \quad V_1 \ll I_C R_N. \tag{11}$$

Before substitution of Eq. (11) into the expression for the supercurrent it is convenient to expand Eq. (6) into Fourier series

$$I(\varphi) = I_0 \Psi(\varphi) = I_0 \sum_{m=1}^{\infty} b_m \sin(m\varphi). \tag{12}$$

In the symmetrical case ($\gamma_- = 0$) it is possible to find the analytical expressions for the Fourier coefficients in Eq. (12)

$$b_m = (-1)^{m+1} \frac{8\sqrt{2}}{\pi} \frac{m}{4m^2 - 1}. \tag{13}$$

For arbitrary values of the asymmetry parameter the coefficients have to be defined numerically and are shown in Fig. 8. It is clearly seen that the larger is the asymmetry parameter γ_- the sharper is the decrease of the Fourier coefficients with the harmonic number m. Practically, for γ_- larger than 0.4 the two first harmonics are sufficient to describe the $I(\varphi)$ relation.

After substitution of Eq. (11) into Fourier series (12)

$$I(\varphi) = I_0 \Psi(\varphi) = I_0 \sum_{m=1}^{\infty} b_m \sum_{k=-\infty}^{\infty} J_k\left(\frac{2\pi V_1}{\Phi_0 \omega} m \right) \times \sin\left(\left(\frac{2\pi V_0}{\Phi_0} m + k\omega \right) t + k\alpha + \varphi_0 \right) \tag{14}$$

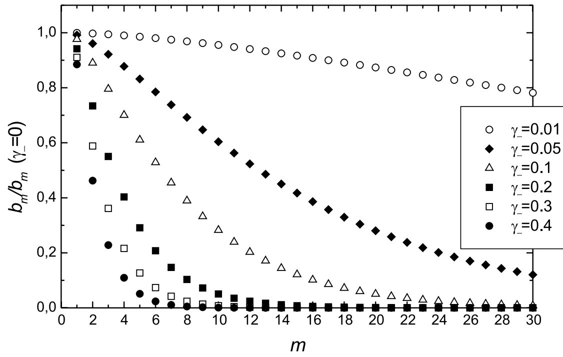

Fig. 8. Dependence of normalized coefficients in Fourier series (12) on the number of harmonics for different values of the asymmetry parameter γ_- calculated for double-barrier junctions in the limit $T \ll T_C^*$.

we can easily see that at $V_{0n,m} = (nm)\omega\Phi_0 / 2\pi$, where n is integer, there are the dc components in Eq. (14).

$$\Delta I_{m,k} = I_C |b_m J_k(2\pi V_1 m/\Phi_0\omega)|. \tag{15}$$

These are the well-known Shapiro steps. At $V_0 = 0$ from Eqs. (11) and (12) for the zeroth order Shapiro step we get

$$I_C(V_1) = I_0 \sum_{m=1}^{\infty} b_m J_0\left(\frac{2\pi V_1}{\Phi_0 \omega} m\right). \tag{16}$$

From Eqs. (15) and (16) it follows that from the amplitude of subharmonic Shapiro steps it is possible to extract the values of coefficients b_m and making use of Fig. 8 to estimate the degree of asymmetry in double-barrier devices.

It is obvious that with increasing temperature the deviation from the classical sinusoidal $I_S(\varphi)$ dependence should decrease but at $T = T_C^*$ it is still appreciable.

5.2. Temperatures in the range of critical temperature of the Al interlayer

If the suppression parameter γ_{eff} is sufficiently large, there is the temperature interval [5] where

$$|T - T_C^*| \leqslant T_C^* \left[\frac{\sqrt{T_C(T_C - T_C^*)}}{\gamma_{\text{eff}} T_C^*}\right]^{2/3}. \tag{17}$$

The term proportional to in the left-hand side of self-consistency equation (4) can be neglected resulting in

$$\frac{I(\varphi)R_N}{2\pi T_C} = \frac{1}{\gamma_{\text{eff}}^{1/3}} \frac{T}{T_C} \sum_{\omega} \frac{f}{\omega\sqrt{\omega^2 + f^2}} \left[\frac{S_1}{S_2}\right]^{1/3} \times \frac{\sin(\varphi)}{(\eta(\varphi))^{2/3}} = I_1 \Psi_1(\varphi), \tag{18}$$

$$\Psi_1(\varphi) = \frac{\sin(\varphi)}{(\eta(\varphi))^{2/3}},$$

where

$$S_1 = 2\pi T \sum_{\omega} \frac{\pi T_C f}{\omega\sqrt{\omega^2 + f^2}}, \qquad S_2 = 2\pi T \sum_{\omega} \frac{1}{\omega^3}.$$

Using the analytical expression for $I(\varphi)$ we can analyze the behavior of double-barrier structures in an external magnetic field and under microwave irradiation.

5.2.1. Fraunhofer pattern

Following the procedure described in Section 5.1.1 for $I_C(H)$ we can obtain

$$\frac{I_C}{I_0} = \frac{\sin(h)}{h} \Theta_1(q, h), \tag{19}$$

with

$$\Theta_1(q,h) = \frac{6}{\sqrt{2(1+\gamma_-^2)}} \times [\sin(q+H)(1 + k\cos(q+h)\cos(h))] \times \Big[(1+k\cos q)^{4/3} + (1+k\cos q)^{2/3} + (1+k\cos(q+2h))^{2/3} + (1+k\cos(q+2h))^{4/3}\Big]^{-1},$$

where parameter q is the root of the following equation

$$\sin(q+2h) = \sin(q)\left[\frac{1+k\cos(q+2h)}{1+k\cos(q)}\right]^{1/3}. \tag{20}$$

It is easy to check that in the asymmetric case ($\gamma_- = 1$, $k = 0$) from Eq. (20) it follows that $\cos(q+h) = 0$ and expression (19) reduces to the well-known Fraunhofer pattern. At arbitrary

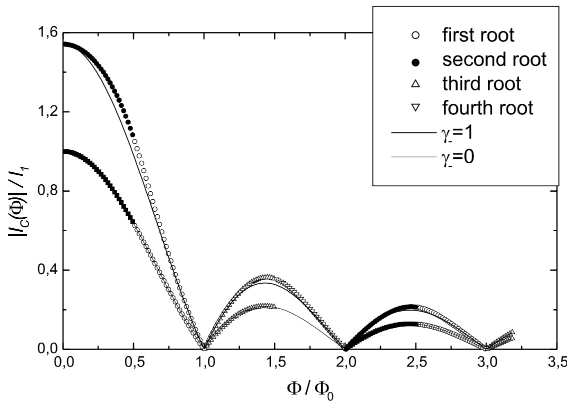

Fig. 9. Magnetic field dependence of critical current calculated numerically for the temperatures close to the critical temperature of the interlayer Al from Eqs. (19) and (20), for different values of the asymmetry parameter γ_-. Small deviations from the Fraunhofer pattern are found in the symmetric case.

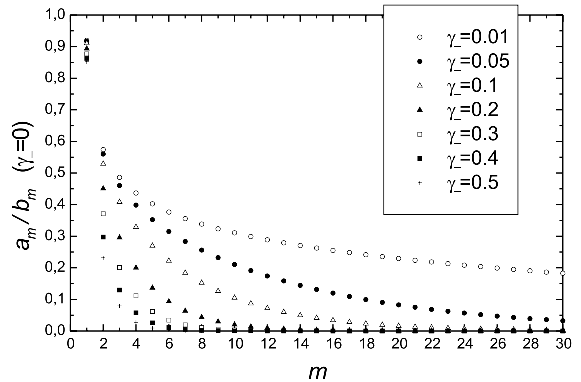

Fig. 10. Dependence of normalized coefficients in Fourier series (21) on the number of harmonic for different values of the asymmetry parameter γ_- calculated for double-barrier junctions in the limit $T \approx T_C^*$.

values of the asymmetry parameter γ_- Eq. (20) has six solutions and $I_C(H)$ has to be composed of them as shown in Fig. 9.

There is a noticeable difference between the results illustrated in Figs. 7 and 9. The most important difference, shown in Fig. 9, is the absence of the solution corresponding to the "0–π–0" state. This result is obvious. In the temperature interval (17) the superconducting order parameter is too weak to be influenced by the S′-electrodes and only the "0–0–0" state is stable in this structures. There is also a small difference in the shape of the $I_C(H)$ dependence, but it is too small to be used for experimental estimation of the asymmetry parameter γ_-.

5.2.2. Shapiro steps

In the temperature interval (17) the $I(\varphi)$ relationship (18) can be also expanded into Fourier series

$$I(\varphi) = I_1\Psi_1(\varphi) = I_1\sum_{m=1}^{\infty} a_m \sin(m\varphi). \qquad (21)$$

The Fourier coefficients a_m have been calculated numerically and are shown in Fig. 10 as a function of m. Even in the symmetric case $(\gamma_- = 0) a_m$ decreases more rapidly with m compared to coefficients b_m defined by formula (13). Nevertheless, at least for the junctions with relatively small asymmetry, it may be possible to estimate γ_- by comparing the coefficients a_m, which are experimentally defined from the amplitude of subharmonic Shapiro steps, with the calculated values shown in Fig. 10.

6. Non-stationary properties

Non-stationary properties of double-barrier junctions are well understood in the case when one of electrodes is in the normal state (SININ′) [23,24]. Various types of non-equilibrium quasiparticle distributions in the interlayer that lead to excess current or current deficit in IVC were studied in various parameter ranges. Processes in SINIS Josephson junctions are more complex due to the time dependence of the superconducting phase difference and multiple Andreev reflections (MAR). A recent review is given in Ref. [25].

The unified approach to the theory of non-stationary processes in SINIS junctions at arbitrary barrier transparency and voltage is not developed yet. In this paper we will describe the theoretical approach applicable to several important limiting cases: high barrier transparency, the regime of low voltages $V \ll \Delta$ and high voltages $V \gg \Delta$. Although it does not cover the full range of phenomena in SINIS junctions, it provides a basis for

understanding the physical processes in these structures. A more detailed study will be presented elsewhere.

6.1. High barrier transparency $\gamma_{eff} \ll 1$

It was shown in Ref. [19] that in this regime the junction is characterized by an universal distribution of the transmission eigenvalues. Then the non-stationary current can be calculated by the MAR technique [26,27] and a further integration over this distribution. The results of calculations of the dc current component were discussed in Ref. [19]. They show an excess current at high bias as well as a subharmonic structure due to MAR. Here we present the first Fourier-harmonics of ac components calculated with the same method.

In Fig. 11 the results of calculations of the voltage dependence for the $\cos\varphi$ and $\sin\varphi$ current components are presented. The subharmonic structure at $eV = 2\Delta/n$ is clearly visible. Since the bias voltage is assumed constant in time, the phase difference $\varphi = 2eVt$ evolves linearly with t, thus both components do not contribute to the dc current.

6.2. Low barrier transparency $\gamma_{eff} \gg 1$

In the regime of low voltages $V \ll \Delta$ the phase difference across the junction $\varphi = 2eVt$ varies slowly in time and the adiabatic approach can be applied. In this case the theory is simplified and coupled diffusion kinetic equations in N metal have the form [25]

$$\frac{\partial}{\partial x}(D_{\rm T}\frac{\partial}{\partial x}f_{\rm T}) + {\rm Im}J_{\rm E}\frac{\partial}{\partial x}f_{\rm L} = 0,$$
$$\frac{\partial}{\partial x}(D_{\rm L}\frac{\partial}{\partial x}f_{\rm L}) + {\rm Im}J_{\rm E}\frac{\partial}{\partial x}f_{\rm T} = 0, \quad (22)$$

where the distribution function $f = f_{\rm L} + \tau_3 f_{\rm T}$, and the generalized diffusion coefficients are

$$D_{\rm T}(E,t) = \frac{1}{4}{\rm Tr}\left[1 - G^{\rm R}\tau_3 G^{\rm A}\tau_3\right] = ({\rm Re}g)^2 + ({\rm Re}f)^2, \quad (23a)$$

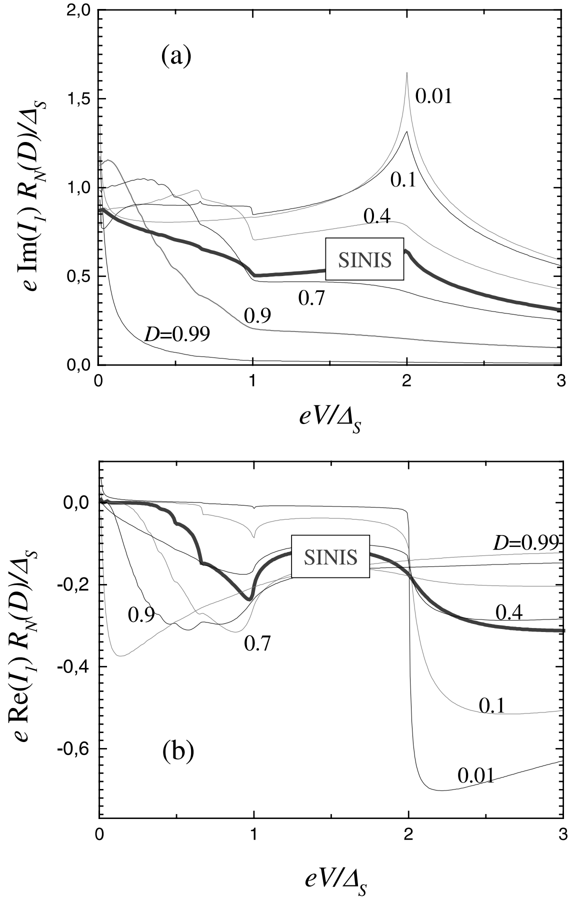

Fig. 11. The ac components (cosinus-term (a) and sinus-term (b)) of the non-stationary current in a SINIS junction in the coherent regime $\gamma_{\rm eff} \ll 1$ and low temperature $T \ll \Delta$ calculated by MAR technique.

$$D_{\rm L}(E,t) = \frac{1}{4}{\rm Tr}\left[1 - G^{\rm R}G^{\rm A}\right] = ({\rm Re}g)^2 - ({\rm Re}f)^2. \quad (23b)$$

Here $G^{\rm R,A}$ are retarded (advanced) 2×2 matrix Green's functions, τ_3 is the Pauli matrix and g, f are normal and anomalous scalar retarded Green's functions.

The spectral supercurrent is given by equation

$${\rm Im}J_{\rm E}(E,t) = \frac{1}{4}{\rm Tr}\left[\tau_3\left(G^{\rm R}\frac{\partial}{\partial_x}G^{\rm R} - G^{\rm A}\frac{\partial}{\partial_x}G^{\rm A}\right)\right]. \quad (24)$$

The total time-dependent current is given by the sum of quasiparticle (dissipative) and pair components:

$$I(t) = I_n + I_s = \frac{1}{R_N}\int_{-\infty}^{\infty}\left\{D_T(E,t)\frac{\partial}{\partial x}f_T(E,t) + \mathrm{Im}J_E(E,t)f_L(E,t)\right\}dE. \quad (25)$$

The distribution functions in the interlayer are determined from the boundary conditions at the barriers $x_{1,2} = \pm d/2$

$$\begin{aligned}\gamma_{B1,2}D_L\frac{\partial}{\partial x}f_{1,2L} &= \pm M_{1,2L}(f_{L0} - f_{1,2L}),\\ \gamma_{B1,2}D_T\frac{\partial}{\partial x}f_{1,2T} &= \pm M_{1,2T}(f_{T0} - f_{1,2T}),\end{aligned} \quad (26)$$

where

$$M_{1,2L(T)} = M_{L(T)}(\pm d/2), \quad f_{1,2L(T)} = f_{L(T)}(\pm d/2),$$

$$M_{T,L} = \mathrm{Re}\,G_s\,\mathrm{Re}\,G \pm \mathrm{Re}F_s\,\mathrm{Re}F\cos(\chi_{1,2} - \chi).$$

Here $\chi_{1,2}$ are the phases of the superconducting electrodes ($\varphi = \chi_1 - \chi_2$) and χ is the phase of the interlayer. The expressions for the phases χ and the functions G, F in the interlayer follow from an analytical continuation of the static solutions, discussed earlier in Refs. [3–5], from the discrete Matsubara frequencies $\omega_n = \pi T(2n+1)$ on the real energy axis E according to $\omega_n = -iE$.

In the considered case $\gamma_{\mathrm{eff}} \gg 1$ the distribution functions in the interlayer are given by

$$\begin{aligned}f_T &= \frac{1}{2}\frac{\gamma_{B2}M_{1T} - \gamma_{B1}M_{2T}}{\gamma_{B2}M_{1T} + \gamma_{B1}M_{2T}} \times\left[\tanh\frac{E+V/2}{2T} - \tanh\frac{E-V/2}{2T}\right],\\ f_L &= \frac{1}{2}\left[\tanh\frac{E+V/2}{2T} + \tanh\frac{E-V/2}{2T}\right].\end{aligned} \quad (27)$$

The quasiparticle current is given by the expression

$$\begin{aligned}I_n(t) &= \frac{1}{R_N}\int_{-\infty}^{\infty}dE\,D_T(E,t)\frac{\partial}{\partial_x}f_T(E,t)\\ &= \frac{1}{R_N}\int_{-\infty}^{\infty}dE\frac{\gamma_{B1}+\gamma_{B2}}{\gamma_{B1}/M_{1T} + \gamma_{B2}/M_{2T}} \times\left[\tanh\frac{E+V}{2T} - \tanh\frac{E-V}{2T}\right].\end{aligned} \quad (28)$$

It follows from Eq. (28) that the quasiparticle current has in general a phase-dependent contribution through the coefficients $M_{1,2T}$. Since the phase difference $\varphi = 2eVt$, the quasiparticle current is time dependent, the dc component is determined by time-averaging. The supercurrent component is given by

$$\begin{aligned}I_s(t) &= \frac{1}{R_N}\int_{-\infty}^{\infty}dE\,\mathrm{Im}J_E(E,t)f_L(E,t)\\ &= \frac{1}{R_N}\int_{-\infty}^{\infty}dE\,\mathrm{Im}J_E(E,t) \times\left[\frac{1}{2}\left(\tanh\frac{E+V/2}{2T} + \tanh\frac{E-V/2}{2T}\right)\right].\end{aligned} \quad (29)$$

In relevant limits the results of the above approach agree with the previous studies of non-equilibrium effects in double-barrier junctions [28–30], while in the present case the phase-coherent effects are also taken into account. Below we shall present the results of calculations of the quasiparticle current component only. In the light of our study of the influence of barrier transparency we investigate the influence of asymmetry on the dc current component and in particular on the behavior of the current deficit at high voltages $V \gg \Delta$. The formalism described above is also valid in this voltage range.

Fig. 12 shows the results of calculations of the dc current component in a SINIS junction for various asymmetry ratios. It is seen that the current deficit at high voltages is present, which is a signature of the non-equilibrium state. The role of asymmetry is quite pronounced here: the current deficit decreases as a function of γ_- from the value 4/3 for symmetric structure (which is just twice a value for a SININ′ junction calculated in [23,24]) to the value 1 for extremely asymmetric junction. Note that we still consider the situation when both barriers are high ($\gamma_{B1}, \gamma_{B2} \gg 1$), therefore the crossover to a SINS junction without current deficit does not take place.

The above results have important consequences for experiments with SINIS junctions. However, a quantitative comparison is not possible at the present stage, in particular since most measurements were performed only at low bias and the

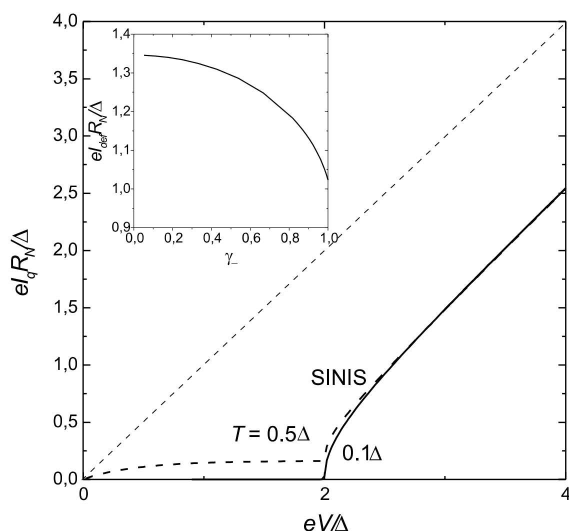

Fig. 12. Quasiparticle dc component of a non-stationary current in a SINIS junction in the regime $\gamma_{\text{eff}} \gg 1$ at low temperature $kT \ll \Delta$. Inset: current deficit as function of barrier asymmetry.

current deficit cannot be determined from the data. Interplay between the features on I–V's at $eV = \Delta$ and $eV = 2\Delta$ is another unresolved question. Interesting experiments in this direction have been reported very recently in Ref. [31]. In this paper the role of barrier asymmetry in SINIS junctions was clear, while a quantitative interpretation remains open. The results of a more detailed study of the theoretical model and the comparison with available data will be a subject of a forthcoming paper.

7. Conclusion

The results of the experimental study of the influence of the barrier transparency on critical current, I_C, and normal resistance, R_N, of the double-barrier Nb/Al_2O_3/Al/Al_2O_3/Nb Josephson junctions are presented. The junctions were fabricated with the conventional process. We have demonstrated that the barrier asymmetry, an important parameter in the technological process, can be determined using the available theoretical models. The comparison of the data with the theoretical model for stationary supercurrent is presented. The general theoretical approach to a study of the non-stationary properties is presented and the results are given for several parameter regimes.

Acknowledgements

The work was supported in part the Russian State Contract No. ΦTH-20(00)-Π, ISTC (Project No. 1199), and INTAS (Project No. 97-1712) and German DFG Project No. Si 704/1-1.

References

[1] V. Patel, S.K. Tolpygo, W. Chen, J.E. Lukens, Extended Abstracts ISEC-99, Berkley, USA, 1999, 229.
[2] V. Patel, J.E. Lukens, IEEE Trans. Appl. Supercond. 9 (1999) 3247.
[3] M.Yu. Kupriyanov, V.F. Lukichev, Sov. Phys. JETP 67 (1988) 1163.
[4] A.V. Zaitsev, Physica C 185–189 (1991) 2539.
[5] M.Yu. Kupriyanov, A. Brinkman, A.A. Golubov, M. Siegel, H. Rogalla, Physica C 326–327 (1999) 16.
[6] L. Capogna, M.G. Blamire, Phys. Rev. B 53 (1996) 5683.
[7] I.P. Nevirkovets, T. Doderer, A. Laub, M.G. Blamire, J.E. Evetts, J. Appl. Phys. 80 (1996) 2321.
[8] I.P. Nevirkovets, J.E. Evettes, M.G. Blamire, Z.H. Barber, E. Goldobin, Phys. Lett. A 232 (1997) 299.
[9] I.P. Nevirkovets, Phys. Rev. B 56 (1997) 832.
[10] L. Capogna, G. Burnell, M.G. Blamire, IEEE Trans. Appl. Supercond. 7 (1997) 2415.
[11] M. Maezawa, A. Shiji, Appl. Phys. Lett. 70 (1997) 3603.
[12] H. Sugiyama, A. Yanada, M. Ota, A. Fujimaki, H. Hayakawa, Jpn. J. Appl. Phys. 36 (1997) L1157.
[13] N. Schulze, R. Behr, F. Muller, J. Niemeyer, Appl. Phys. Lett. 73 (1998) 996.
[14] H. Schulze, F. Müller, R. Behr, J. Kohlmann, J. Niemeyer, D.Balashov, IEEE Trans. Appl. Supercond. 9 (1999) 4241.
[15] D. Balashov, F.-Im. Buchholz, H. Schulze, M.I. Khabipov, W. Kessel, J. Niemeyer, Supercond. Sci. Technol. 11 (1999) 1401.
[16] D. Balashov, M.I. Khabipov, F.-Im. Buchholz, W. Kessel, J. Niemeyer, Supercond. Sci. Technol. 11 (1999) 1.
[17] P. Nevirkovets, J.B. Ketterson, S. Lomatch, Appl. Phys. Lett. 74 (1999) 1624.
[18] D. Balashov, F.-Im. Buchholz, H. Schulze, M.I. Khabipov, R. Dolata, M.Yu. Kupriyanov, J. Niemeyer, Supercond. Sci. Technol. 13 (2000) 244.
[19] A. Brinkman, A.A. Golubov, Phys. Rev. B 61 (11) (2000) 297.
[20] H. Schulze, R. Behr, J. Kohlmann, F. Müller, J. Niemeyer, Supercond. Sci. Technol., submitted for publication.

[21] H.A. Huggins, M. Gurvitch, J. Appl. Phys. 57 (1985) 2103.
[22] A.A. Golubov, E.P. Houwman, J.G. Gijsbertsen, V.M. Krasnov, J. Floksra, H. Rogalla, M.Yu. Kupriyanov, Phys. Rev. B 51 (1995) 1073.
[23] A.V. Zaitsev, JETP Lett. 51 (1990) 41.
[24] A.F. Volkov, A.V. Zaitsev, T.M. Klapwijk, Physica C 210 (1993) 21.
[25] W. Belzig, F.K. Wilhelm, C. Bruder, G. Schoen, A.D. Zaikin, Superlat. Microstruct. 25 (1999) 1251.
[26] D.V. Averin, A. Bardas, Phys. Rev. Lett. 75 (1995) 1831.
[27] D.V. Averin, A. Bardas, Phys. Rev. B 56 (1997) R8518.
[28] M.G. Blamire, E.C.G. Kirk, J.E. Evetts, T.M. Klapwijk, Phys. Rev. Lett. 66 (1991) 220.
[29] D.R. Heslinga, T.M. Klapwijk, Phys. Rev. B 47 (1993) 5157.
[30] A.V. Zaitsev, JETP Lett. 55 (1992) 66.
[31] I.P. Nevirkovets, J.B. Ketterson, S.E. Shafranjuk, S. Lomatch, Phys. Lett. A 269 (2000) 238.